Supporting Information

Efficient and stabilized molecular doping of hole-transporting materials driven by a cyclic-anion strategy for perovskite solar cells

Correspondence to: luojs@uestc.edu.cn

Table of Contents

1. Materials

FAI (99.8%), PbI_2 (99.999%) and ITO glass were purchased from Advanced Election Technology CO., Ltd. PTAA (99.9%), *t*-BP (99%), Li-TFSI (99%), $PbBr_2$ (99.9%), MABr (99.8%) and CsBr (99.9%) were purchased from Xian Yuri Solar Co.,Ltd. Li-CYCLIC (98%) was purchased from TCI. The SnO_2 (15 wt%) was purchased from Alfa Aesar. The N, N-dimethylformamide (DMF), dimethyl sulfoxide (DMSO), chlorobenzene, ethanol and acetonitrile were purchased from Sigma-Aldrich. All the materials were used as received without any purification.

2. Characterization

The electron spin resonance spectroscopy (ESR) was analyzed by a Bruker-E500 spectrometer. The ultraviolet-visible absorption spectrum (UV-vis) was measured by a Hitachi UV-visible spectrophotometer (U-2910). The ultraviolet photoelectron spectroscopy (UPS) measurements were performed by the AXIS ULTRA DLD instrument from Kratos, UK, using a HeI monochromator with 21.22 eV source energy. The steady-state fluorescence spectroscopy (PL) was collected by a Hitachi spectrophotometer (F-4600). The transient fluorescence spectra (TRPL) were measured at room temperature using the time-correlated single photon counting (TCSPC) technique with a FluoroLog-3 modular spectrofluorometer (HORIBA Jobin Yvon). The electrochemical impedance spectroscopy (EIS) of the PSCs under ambient air

was recorded by an electrochemical workstation (CHI 660E, Shanghai, Chenhua) and a solar simulator (Zolix Instrument Co., Ltd. Beijing). The surface and cross-sectional morphology of the perovskite films were observed by a scanning electron microscopy (JEOL JSM-7600F). The *J-V* curve of the PSCs was measured at room temperature using an electrochemical workstation (CHI 660E, Shanghai, Chenhua) under AM 1.5G simulated solar light (100 mW cm-2), and the incident light intensity was calibrated with a standard silicon solar cell. The incident photon-to-electron conversion efficiency (IPCE) spectra were performed by using a IPCE measurement system (QTest Station 2000, CROWNTECH, USA). Regarding the environmental stability of the PSCs, the devices were kept at ambient conditions (50-85% room humidity and room temperature) in a dark environment for 40 days. Regarding the working stability of PSCs, unencapsulated PSCs were continuously tested in a standard simulated sunlight, room temperature and N_2 atmosphere. The water contact angle of the films was examined by a droplet shape analyzer (Krüss DSA100). The atomic force microscopy (AFM) measured by Bruker Dimension Icon AFM instrument. The two-dimensional grazing incidence X-ray diffraction (2D-GIXD) images were conducted at the BL14B1 experimental station of Shanghai Synchrotron Radiation Center with an incident angle of 0.16° and an exposure time of 30 s. After the devices were heated at 85 °C for 16 hours, the time-of-flight secondary ion mass spectrometry (TOF-SIMS) was measured using the ION TOF-SIMS 5 instrument.

3. DFT calculations

The calculations of optimized structures, relaxed models and electron transfer were performed by the CP2K[1] program using the spin-polarized density functional.[2, 3] All calculations used a mixed Gaussian and planewave basis sets. Norm-conserving Goedecker-Teter-Hutter pseudopotentials were used to represent core electrons.[4-6] The van der Waals correction of Grimme's DFT-D3 model was adopted.[7] The exchange-correlation functional employed was the Perdew, Burke, and Enzerhof (PBE)[8] generalized gradient approximation. The wavefunction of the valence electrons was expanded using a double-zeta basis set incorporating polarization functions[9], with an auxiliary plane wave basis set with an energy cutoff of 360 eV. The configuration was optimized using the Broyden-Fletcher-Goldfarb-Shanno (BGFS) algorithm, with a SCF convergence criteria of 1.0×10^{-6} au.

The calculations of ESP, PDOS and differential charge maps were performed by the Gaussian 09W program using the B3LYP exchange-correlation functional. The calculation of electron exchange-correlation interactions using the GGA-PBE exchange functional for generalized gradient approximation in the Dmol3 program.[10] For perovskite, in order to simplify the calculation, the $CH_3NH_3PbBr_3$ perovskite model with a stable (001) surface was used to simulate the trap state. A 20 Å vacuum layer was set, the Monkhorst-Pack point grid was set to 2×2×1, and the cutoff energy was 600 eV.

4. Precursor solution and device fabrication

The ITO glass substrates were ultrasonically cleaned with deionized water, acetone, and ethanol in sequence, each step was more than 30 minutes, and dried with a nitrogen flow, then treated with UV-ozone for 20 minutes. All the solutions were passed through a 0.22-mmfilter before use. The SnO_2 solution was prepared by diluting 15 wt% SnO_2 aqueous solutions (600 μL) with 3 mL of isopropanol/H_2O (1/1, v/v). The SnO_2 solution was spin coated onto an ITO substrate at 4000 rpm for 40 s, and annealed in ambient air at 150 °C for 30 min. 1.2 M $MA_{0.10}Cs_{0.05}FA_{0.85}Pb(I_{0.95}Br_{0.05})_3$ perovskite precursor solution was prepared in mixture solvent of DMF and DMSO (4:1, v/v). The perovskite solution was spin coated with three steps program at 200, 2000 and 4000 rpm for 3, 10 and 25 s, respectively. During the third step, chlorobenzene was poured on the spinning substrate as antisolvent. The spin-coated perovskite precursor films were sequentially heated at 100 and 150 °C. For the control PTAA: Li-TFSI solution, dissolved 15 mg PTAA in 1 mL of chlorobenzene, added 7.5 μL of bis(trifluoromethane)sulfonamide lithium salt (Li-TFSI)/acetonitrile (170 mg/mL) and 7.5 μL of *t*-BP/acetonitrile (1:1 v/v). The PTAA (15 mg) and Li-CYCLIC were dissolved into 1 mL CB and mixed by desired Li-CYCLIC/PTAA ratios ranging from 10% to 20% (mole ratio with respect to the repeat unit mass), and *t*-BP was added at a mass ratio of 1:6 to Li-CYCLIC. The HTL solution was spin-coated on the perovskite layer by spin coating at 3000 rpm for 30 s. Finally, Au electrode was thermally evaporated.

5. Figures S1-S13

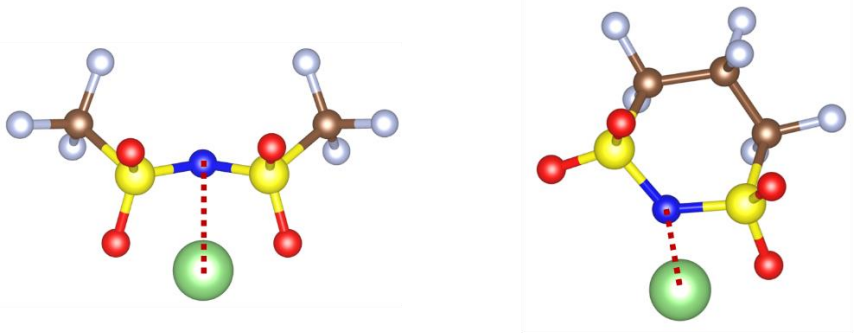

Figure S1. The distance between the Li atom and N atom in the anion.

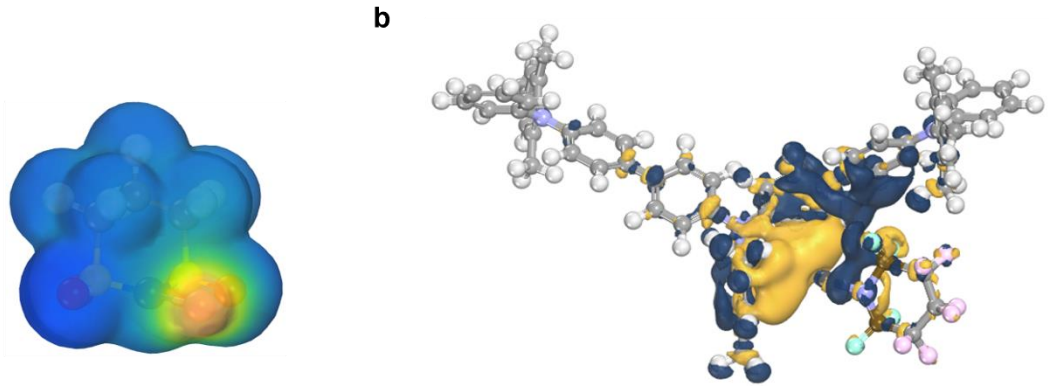

Figure S2. (a) ESP of Li-CYCLIC. (b) Differential charge map of PTAA trimer: Li-CYCLIC (yellow and blue respectively represent the depletion and accumulation of electrons).

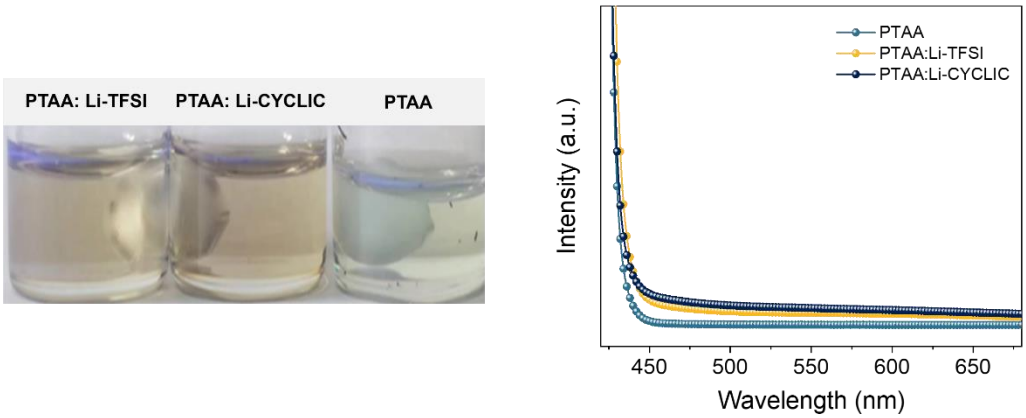

113

114 **Figure S3.** The color change and UV-vis of PTAA, PTAA: Li-TFSI and PTAA:

115 Li-CYCLIC solutions.

116

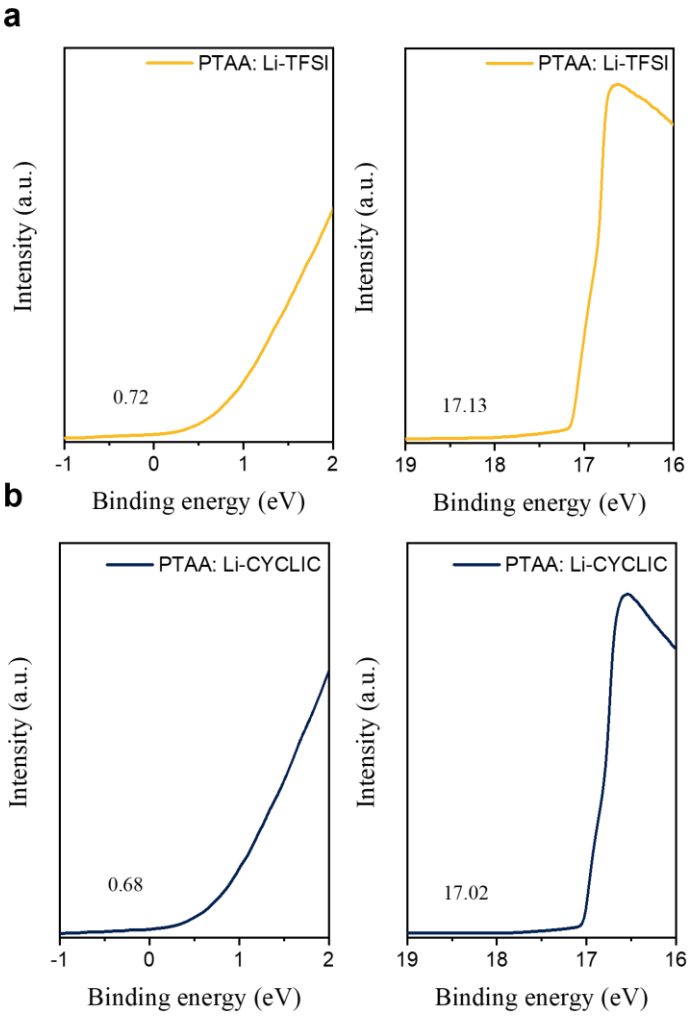

Figure S4. UPS spectra of (a) PTAA: Li-TFSI and (b) PTAA: Li-CYCLIC films, the calculated as follows.

$$W_F = 21.22 - E_{cut\text{-}off}$$

$$\Phi = 21.22 - (E_{cut\text{-}off} - E_i)$$

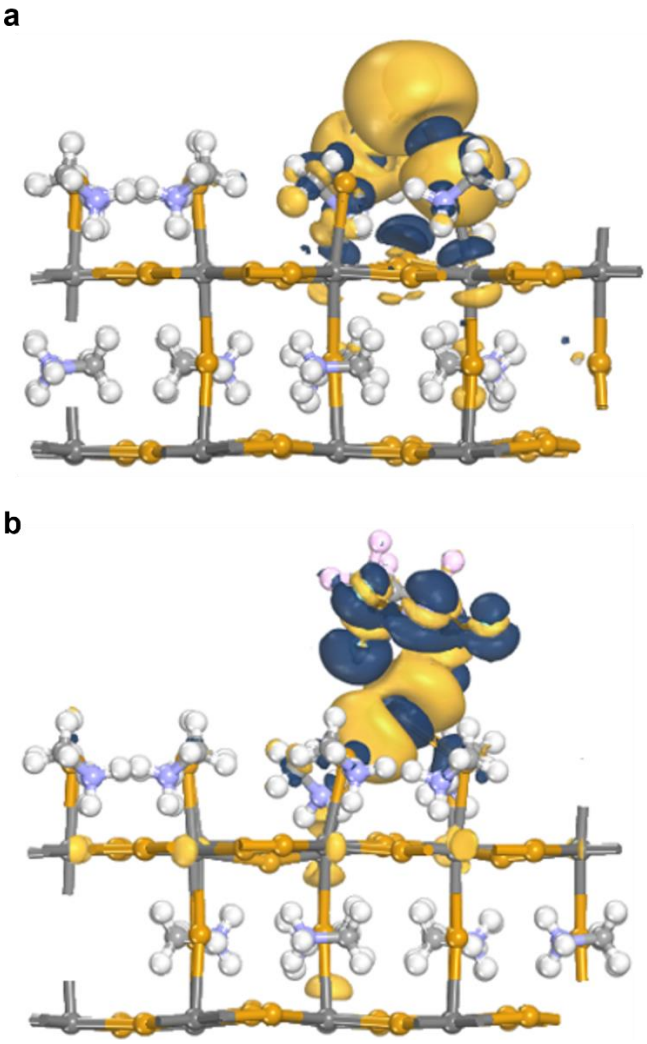

Figure S5. Differential charge map of (a) Pb-Pb dimer defects on the surface of perovskite (001) and (b) the interaction between Li-CYCLIC and Pb-Pb dimer defects (yellow and blue respectively represent the depletion and accumulation of electrons).

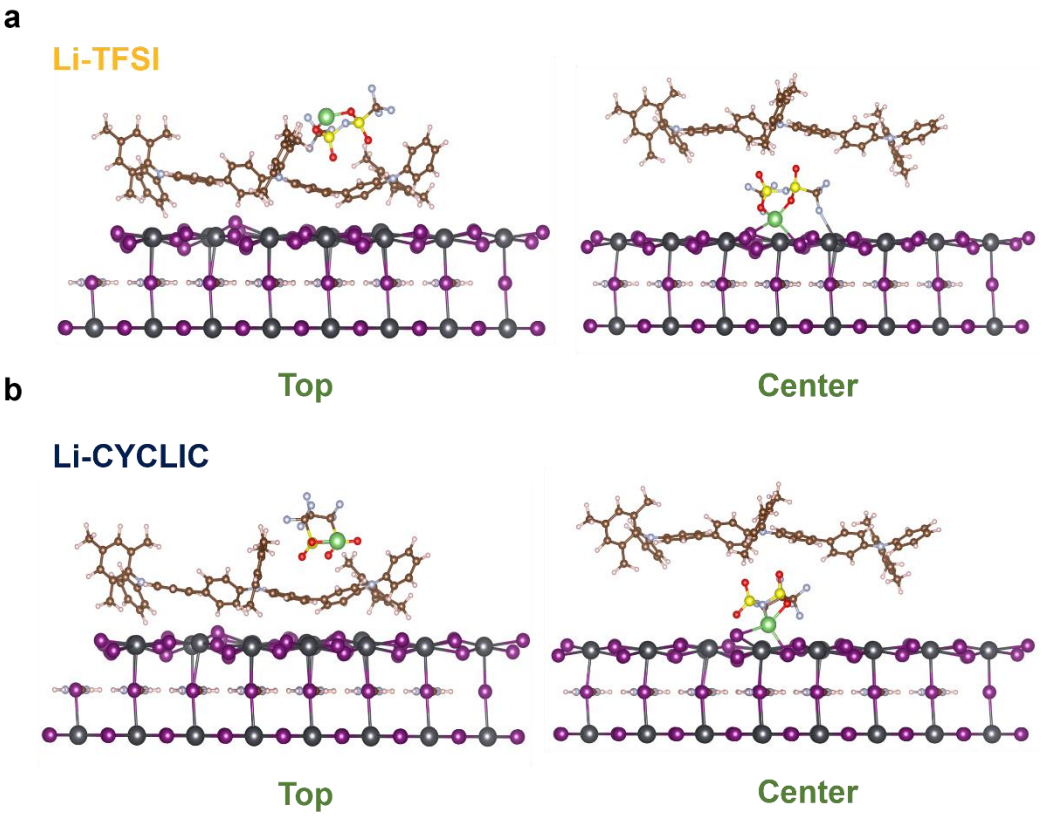

Figure S6. The relaxed models of perovskite and PTAA with (a) Li-TFSI and (b) Li-CYCLIC.

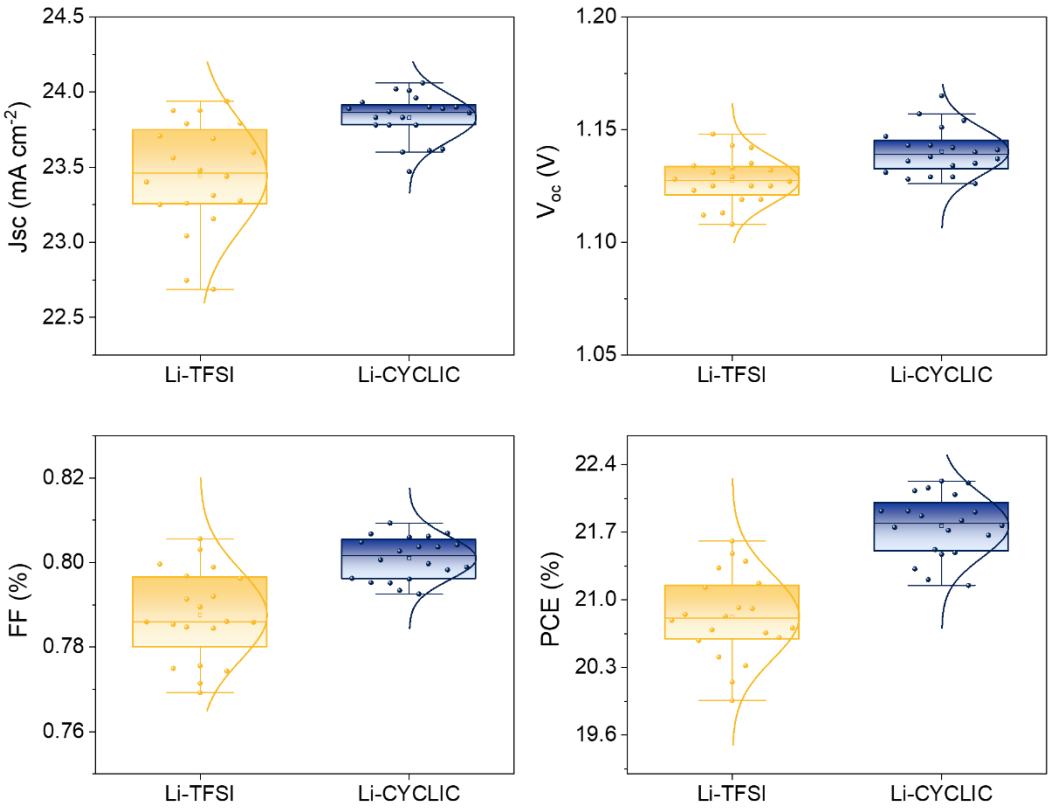

Figure S7. The distribution of photovoltaic parameters for PSCs based on Li-TFSI and Li-CYCLIC.

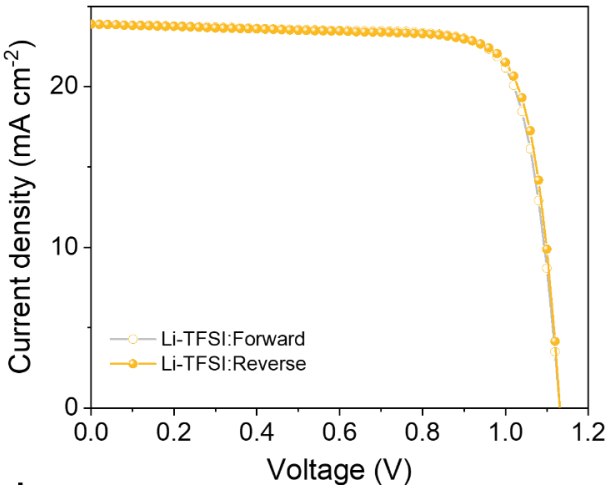

Figure S8. *J-V* curves of PSC based on Li-TFSI under forward and reverse scans.

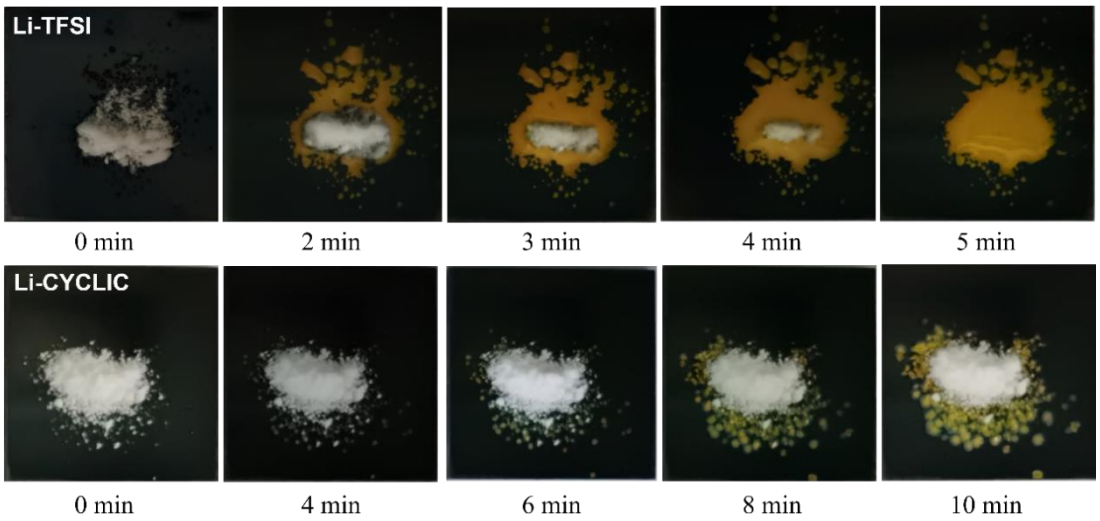

141

142 **Figure S9.** Photos of dopants decomposing perovskite films by absorbing

143 moisture in the air.

144

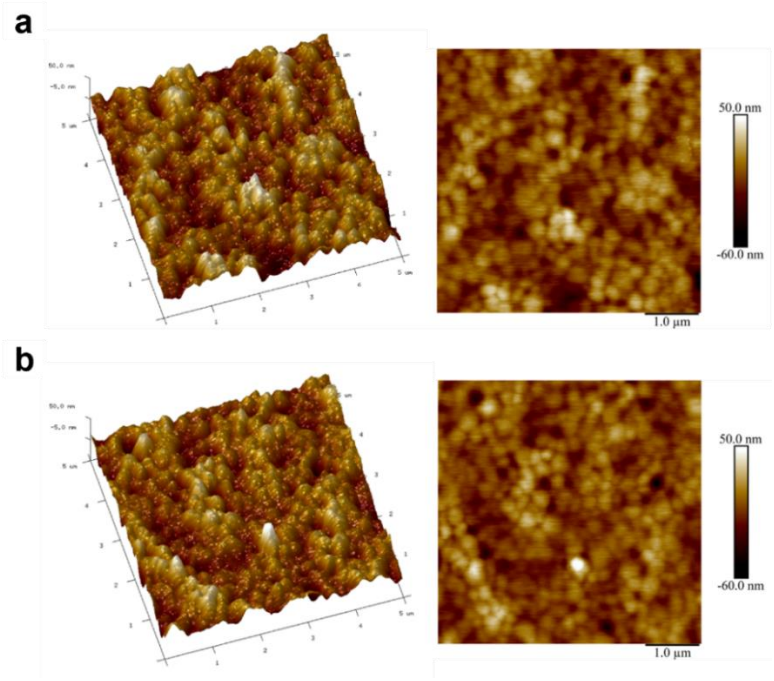

Figure S10. The AFM images of fresh (a) PTAA: Li-TFSI and (b) PTAA: Li-CYCLIC film.

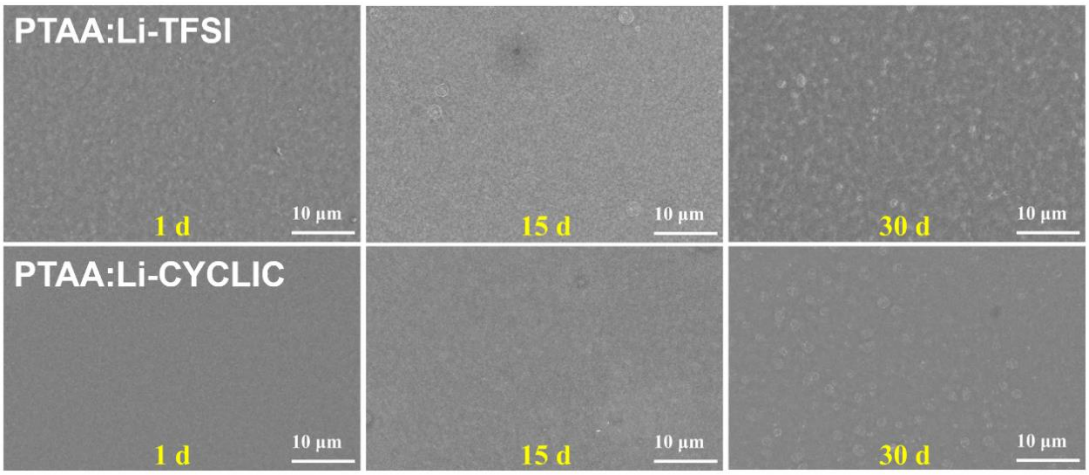

Figure S11. The aged SEM morphology of PTAA: Li-TFSI and PTAA: Li-CYCLIC films.

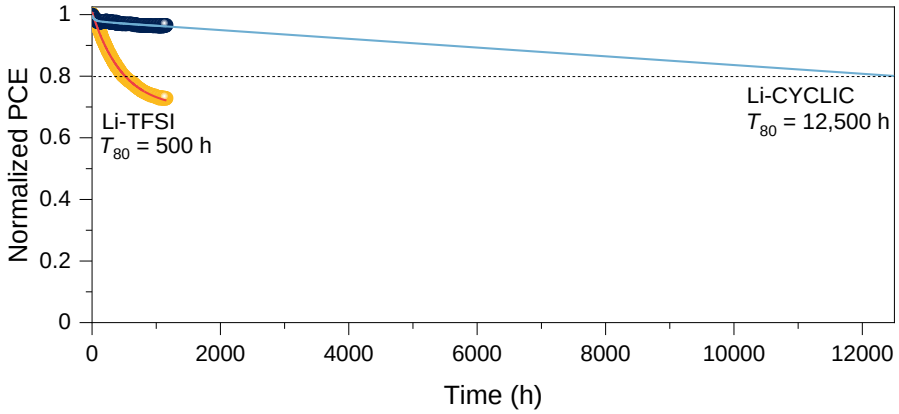

Figure S12. Operational stability and T_{80} lifetime of PSCs based on Li-TFSI and Li-CYCLIC under continuous 1-sun illumination in N_2.

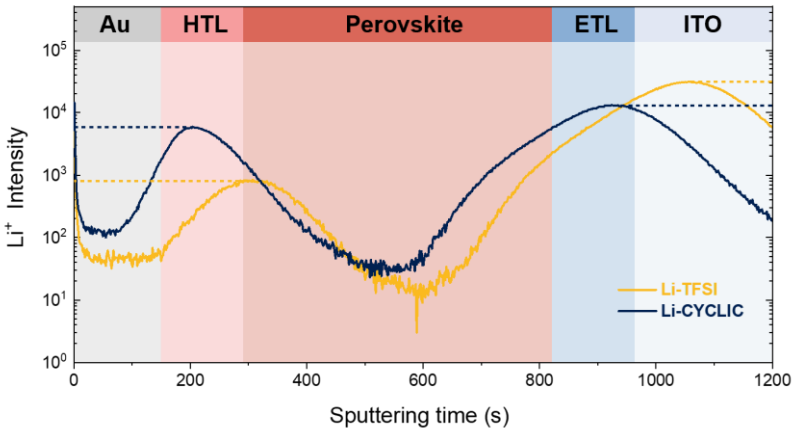

157

158 **Figure S13.** TOF-SIMS results of Li^+ ions in aged devices based on Li-TFSI

159 and Li-CYCLIC.

160

6. Table S1-S6

Table S1. The calculated total energy values of different forms of dopants during the action process.

	Total energy (Hartree)
Li-TFSI	-258.761260
Li-CYCLIC	-264.423085
$PTAA^{\bullet+}$	-423.178764
$TFSI^{-}$	-251.362776
$CYCLIC^{-}$	-257.034427
$PTAA^{\bullet+}TFSI^{-}$	−674.577920
$PTAA^{\bullet+}CYCLIC^{-}$	-680.251864

Table S2. The fitting parameters of TRPL data through an exponential model.

Sample	A_1	τ_1 (ns)	A_2	τ_2 (ns)	τ_{avg} (ns)
Perovskite	0.92	13.02	0.59	227.84	210.22
Perovskite/PTAA: Li-TFSI	1.71	2.71	0.20	33.09	20.21
Perovskite/PTAA: Li-CYCLIC	2.09	2.38	0.18	23.88	12.31

$$y = A_1 \exp\left(-\frac{t}{\tau_1}\right) + A_2 \exp\left(-\frac{t}{\tau_2}\right) + y_0$$

$$\tau_{avg} = \frac{A_1\tau_1^2 + A_2\tau_2^2}{A_1\tau_1 + A_2\tau_2}$$

Table S3. The total energy of the PTAA and perovskite with Li-TFSI and Li-CYCLIC.

Sample	Total energy (Hartree)
Li-TFSI_center	-2815.749836
Li-TFSI_top	-2815.778977
Li-CYCLIC_center	-2821.411495
Li-CYCLIC_top	-2821.429126

Table S4. Photovoltaic parameters of the PSCs based on various molarities of Li-CYCLIC and Li-TFSI.

	J_{SC} (mA/cm^2)	V_{OC} (V)	FF (%)	PCE (%)
10 mol% Li-CYCLIC	23.39	1.132	77.07	20.41
15 mol% Li-CYCLIC	23.96	1.151	80.60	22.23
20 mol% Li-CYCLIC	23.95	1.127	75.61	20.42
Li-TFSI	23.88	1.133	79.89	21.61

Table S5. The average values and the standard deviation of photovoltaic parameters for PSCs based on Li-TFSI and Li-CYCLIC.

	Li-TFSI	Li- CYCLIC
J_{SC} (mA/cm^2)	23.44 ± 0.49	23.83 ± 0.23
V_{OC} (V)	1.127 ± 0.021	1.140 ± 0.017
FF (%)	78.75 ± 1.81	80.10 ± 0.83
PCE (%)	20.82 ± 0.79	21.77 ± 0.46

Table S6. Photovoltaic parameters of the PSCs based on Li-TFSI and 15 mol% Li-CYCLIC under forward and reverse scans.

Dopant	Scan direction	J_{SC} (mA/cm^2)	V_{OC} (V)	FF (%)	PCE (%)
Li-TFSI	Reverse	23.69	1.133	79.89	21.61
	Forward	23.89	1.132	79.21	21.43
15 mol% Li-CYCLIC	Reverse	23.96	1.151	80.60	22.23
	Forward	23.94	1.149	80.70	22.20

References

1. J. VandeVondele, M. Krack, F. Mohamed, M. Parrinello, T. Chassaing and J. Hutter, *Comput. Phys. Commun.*, 2005, **167**, 103-128.
2. P. Hohenberg and W. Kohn, *Phys. Rev.*, 1964, **136**, B864-B871.
3. W. Kohn and L. J. Sham, *Phys. Rev.*, 1965, **140**, A1133-A1138.
4. S. Goedecker, M. Teter and J. Hutter, *Phys. Rev. B*, 1996, **54**, 1703-1710.
5. C. Hartwigsen, S. Goedecker and J. Hutter, *Phys. Rev. B*, 1998, **58**, 3641-3662.
6. M. Krack and M. Parrinello, *Phys. Chem. Chem. Phys.*, 2000, **2**, 2105-2112.
7. S. Grimme, J. Antony, S. Ehrlich and H. Krieg, *J. Chem. Phys.*, 2010, **132**.
8. J. P. Perdew, K. Burke and M. Ernzerhof, *Phys. Rev. Lett.*, 1996, **77**, 3865-3868.
9. J. VandeVondele and J. Hutter, *J. Chem. Phys.*, 2007, **127**.
10. B. Delley, *J. Chem. Phys.*, 2000, **113**, 7756-7764.